Enhanced Autofocus Algorithm Using Robust Focus Measure and Fuzzy Reasoning

Sang-Yong Lee, Yogendera Kumar, Ji-Man Cho, Sang-Won Lee, and Soo-Won Kim

***Abstract*—A new passive autofocus algorithm consisting of a robust focus measure for object detection and fuzzy reasoning for target selection is presented. The proposed algorithm first detects objects distributed in the image using a mid-frequency discrete cosine transform focus measure and then selects the target object through fuzzy reasoning with three fuzzy membership functions. The proposed algorithm is designed as full digital blocks and fabricated using 0.35-μm CMOS technology. Experimental results obtained from various samples show that the present method is insensitive to Gaussian and impulsive noises and able to improve the quality of the image by focusing to the appropriate target object.**

***Index Terms*—Autofocus (AF), focus measure, fuzzy reasoning, object detection.**

I. Introduction

THE autofocus (AF) function has become an integral part of the precapture image-processing stage in modern digital and video cameras. The focus may have to be adjusted when the object or the camera changes its position. Either active AF involving infrared/ultrasound signals or passive AF based on sharpness sensing is used for this propose. Usually, passive AF functions are preferred due to their cost effectiveness and software flexibility [1], [2]. These functions extract the sharpness information from the image to adjust the focus lens and bring it into focus [3], [4]. The entire process includes two stages: the first determines the focus measure which reflects the degree of focus using focus measure operator, and the other is the searching algorithm that finds the best in-focus position. Various focus measure methods have been proposed by the researchers. These include the Sobel gradient method by Tenenbaum [5], bandpass filter-based technique [6], energy of Laplacian (EOL) [7], [8], sum-modified Laplacian (SML) [9], and frequency-selective weighted median (FSWM) filter [10]. In addition to theses, methods based on discrete cosine transform (DCT) and wavelet transform are also developed [11]–[13]. Studies on searching algorithms are also carried out which include Fibonacci [3], mountain climbing servo (MCS) [4], fast hill-climbing search (HCS) [10], and modified fast climbing search with adaptive step size (MFCS) [14]. Sohn *et al.* [1] recently proposed a compact AF function that uses multiple high-pass filters and implemented on system on chip (SOC). This is a good method in terms of accuracy, but has higher hardware complexity and is easily affected by various electrical noises. All of the above studies show satisfactory performance when the main object is in the center evaluation window and the system is in the low noise level. In other cases like: 1) when the object steps aside the center window [Fig. 1(a)]; 2) when the background has a higher frequency than the target object [Fig. 1(b)]; and 3) when multiple objects having different distances appear in the center window [Fig. 1(c)], it is difficult to focus the main object. To resolve these problems, a robust focus measure, namely the midfrequency discrete cosine transform (MF-DCT), which is less affected by various electrical noises, and a passive AF algorithm that is able to detect the target object using fuzzy reasoning [15], [16] are proposed in this study.

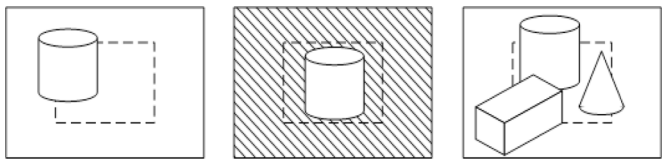

Fig. 1. Frequently occurred focus missing cases.

This paper is organized as follows. Section II provides the brief review of the conventional approaches used for focus measuring. The proposed AF algorithm, which includes three components—focus measure, fuzzy reasoning and searching algorithm—is explained in Section III. Section IV describes the hardware implementation. Experimental results are shown in Section V, and, finally, conclusions are driven in Section VI.

II. Some Approaches to Focus Measure

In general, passive AF algorithms use a focus measuring operator to estimate the sharpness of the image. Based on this approach, the image having a maximum focus measure is considered as the focused one (Fig. 2). Here, a few derivative based focus measuring approaches are briefly reviewed.

A. Tenenbaum Gradient

Proposed by Tenenbaum, it is the most popular AF function based on image differentiation. It convolves an image block $(\mathbf{P})$ with two Sobel operators ($\mathbf{O}_{\mathbf{Sobel.x}}$ and $\mathbf{O}_{\mathbf{Sobel.y}}$) and then

Manuscript received November 17, 2006; revised September 19, 2007. First published April 30, 2008; current version published October 8, 2008. This work was supported by the Ministry of Information and Communication (MIC), Korea, under the IT Foreign Specialist Invitation Program (ITFSIP) supervised by the Institute of Information Technology Assessment (IITA) and Korea IT Industry Promotion Agency (KIPA). This paper was recommended by Associate Editor T. Fujii.

S.-Y. Lee, Y. Kumar, J.-M. Cho, and S.-W. Kim is with the Department of Electronics Engineering, Korea University, Seoul 136–713, Korea (e-mail: sylee@asic.korea.ac).

S.-W. Lee is with Intel Corporation, Hudson, MA 01749 USA (e-mail: sangwon.lee@intel.com).

Color versions of one or more of the figures in this paper are available online at http://ieeexplore.ieee.org.

Digital Object Identifier 10.1109/TCSVT.2008.924105

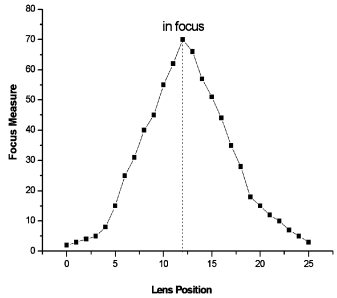

Fig. 2. Focus measure versus lens position.

sums the square of the gradient vector components to calculate the focus measure as

$$\mathbf{O_{Sobel.x}}: \begin{array}{|c|c|c|}\hline -1 & 0 & 1 \\ \hline -2 & 0 & 2 \\ \hline -1 & 0 & 1 \\ \hline \end{array}$$

$$\mathbf{O_{Sobel.y}}: \begin{array}{|c|c|c|}\hline 1 & 2 & 1 \\ \hline 0 & 0 & 0 \\ \hline -1 & -2 & -1 \\ \hline \end{array} \quad (1)$$

$$FM_{\text{Sobel}} = \sum_x \sum_y \Big[\{\mathbf{O_{Sobel.x}} \bullet \mathbf{P}(\mathbf{x},\mathbf{y})\}^2 + \{\mathbf{O_{Sobel.y}} \bullet \mathbf{P}(\mathbf{x},\mathbf{y})\}^2\Big]. \quad (2)$$

B. Sum-Modified Laplacian (SML)

Nayer and Nakagawa proposed a noise-insensitive focus measure based on the SML operators. The modified Laplacian operators ($\mathbf{O_{SML.x}}$ and $\mathbf{O_{SML.y}}$) are given by

$$\mathbf{O_{SML.x}}: \begin{array}{|c|c|c|}\hline 0 & 0 & 0 \\ \hline -1 & 2 & -1 \\ \hline 0 & 0 & 0 \\ \hline \end{array}$$

$$\mathbf{O_{SML.y}}: \begin{array}{|c|c|c|}\hline 0 & -1 & 0 \\ \hline 0 & 2 & 0 \\ \hline 0 & -1 & 0 \\ \hline \end{array} \quad (3)$$

and the focus measure is computed as

$$FM_{SML} = \sum_x \sum_y \Big[|\mathbf{O_{SML.x}} \bullet \mathbf{P}(\mathbf{x},\mathbf{y})| + |\mathbf{O_{SML.y}} \bullet \mathbf{P}(\mathbf{x},\mathbf{y})|\Big]^2. \quad (4)$$

C. Energy of Laplacian (EOL)

Subbarao and Choi proposed some schemes based on the energy of image, the energy of image gradient, and the EOL of the image, respectively. The focus measure computation is performed as

$$FM_{\text{EOL}} = \sum_x \sum_y [\mathbf{O_{SML.x}} \bullet \mathbf{P}(\mathbf{x},\mathbf{y}) + \mathbf{O_{SML.y}} \bullet \mathbf{P}(\mathbf{x},\mathbf{y})]^2. \quad (5)$$

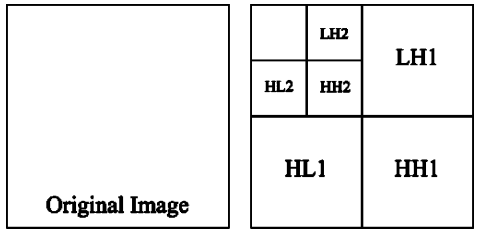

Fig. 3. Decomposition of the wavelet transform.

D. Frequency-Selective Weighted Median (FSWM) Filter

An FSWM filter is a high-pass nonlinear filter based on the difference of medians well known as nonlinear edge detectors that remove the impulsive noise effectively. The FSWM uses several nonlinear subfilters having a weight according to the frequency acting like a bandpass filter as

$$y_F(n) = \sum_{i=1}^{N} \alpha_i \bullet \hat{y}_i(n) \quad (6)$$

where $y_F(n)$ is the FSWM filter, N is the number of subfilters, $\alpha_i \in R$, and $\hat{y}_i(n)$ is the WM filter. The focus measure can be produced by summing FSWM filtering results, F_x and F_y, applied to an image along the horizontal and vertical directions as

$$FM_{\text{FSWM}} = \sum_x \sum_y \left(F_x^2 + F_y^2\right). \quad (7)$$

E. Wavelet Transform

The algorithm proposed by Yang and Nelson uses the Daubechies D6 wavelet filter, applying both high-pass (H) and low-pass (L) filtering to an image. The resultant image is divided into four subimages, LL1, HL1, LH1, and HH1, as shown in Fig. 3. The focus measure is computed by summing the absolute values in the HL1, LH1, and HH1 regions as

$$FM_{\text{WT}} = \frac{1}{w \bullet h}\left[\sum_{x,y} (W_{\text{LH1}}(x,y) - \mu_{LH1})^2 + \sum_{x,y} (W_{\text{HL1}}(x,y) - \mu_{\text{HL1}})^2 + \sum_{x,y} (W_{\text{HH1}}(x,y) - \mu_{\text{HH1}})^2\right] \quad (8)$$

where w and h represent the size of the evaluation window and $W_{\text{LH1}}(x,y)$ and μ_{LH1} are the coefficients set and expectation values of LH1.

III. Proposed AF Algorithm

A. MF-DCT-Based Focus Measure

DCT has shown efficient and robust performance in a focusing image method while possessing a computationally attractive implementation [11]. In the DCT-based focus measure approach, first the image is divided into blocks of $8*8$ pixels and then DCT is applied on each block to transform the pixel information into the DCT domain

$$\begin{aligned} S_{i,j} &= \frac{1}{4}^{*} C_i^* C_j^* \sum_{x=0}^{7}\sum_{y=0}^{7} P_{x,y}^* \\ &\quad \times \cos\left[\frac{(2x+1)^* i^* \pi}{16}\right]^* \cos\left[\frac{(2y+1)^* j^* \pi}{16}\right] \\ C_i &= \frac{1}{\sqrt{2}} \\ C_j &= \frac{1}{\sqrt{2}} \\ C_i &= C_j = 1 \end{aligned} \tag{9}$$

where $C_i = 1/\sqrt{2}$ when $i = 0$, $C_j = 1/\sqrt{2}$ when $j = 0$, and $C_i = C_j = 1$ otherwise. This operation results in a series of 64 coefficients, each representing a particular spatial frequency. These 64 (1 dc and 63 ac) coefficients are then arranged according to their frequencies as shown in Fig. 4. According to Subbarao *et al.* [6], bandpass filters make the focus measure have sharp peaks while generally retaining monotonicity and unimodality. Furthermore, bandpass filters have the characteristic of attenuating low frequencies which contribute less to the focus measure and attenuating high frequencies affected by side lobes and noise, but emphasizing medium frequencies. Keeping in mind the results produced by Subbarao [6], 16 components representing mid and high frequencies are chosen. These 16 components were compared to see their effect on the focus measure for these different types of objects (see Straw, Sand, and Doll in Fig. 14), as shown in Fig. 5. It is obvious from Fig. 5 that components $S_{4,4}$, $S_{4,5}$, and $S_{5,4}$ have larger effects compared with the others. For these comparisons, the size of the evaluation center window is taken as $240*240$ (the center part of the image with size $640*480$). The simulations were done with ten images at different lens positions captured by digital camera. Furthermore, when $S_{4,4}$, $S_{4,5}$, and $S_{5,4}$ were compared with one another, it was found that $S_{4,4}$ needs only three kinds of coefficients for getting results whereas $S_{4,5}$ and $S_{5,4}$ need nine, as shown in Fig. 6. We conclude from the above observations that the signal power of this mid-frequency component ($S_{4,4}$) is taken into account to calculate the focus measure.

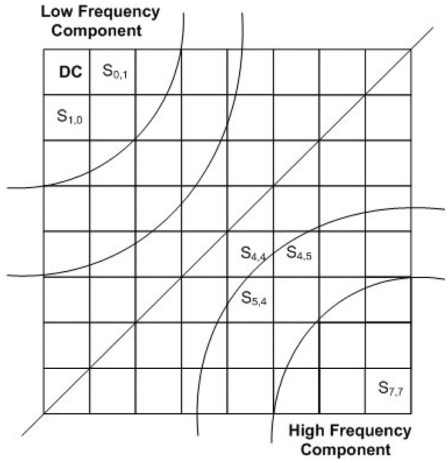

Fig. 4. Frequency distribution of DCT results.

It was recently shown by Malik and Choi [17] that a window size greater than $5*5$ results in two major errors: one is the introduction of blurring and another is the wrong extraction of frame numbers for images corresponding to the sharpest values in the sequence of the image. In addition, a large window size gives rise to larger standard deviation. The standard deviation of the $S_{4,4}$ coefficient is calculated by the method proposed in [7], [8] (10), shown at the bottom of the page, which is larger than the EOL, which was the best measure in [7] and [8]; see (11), shown at the bottom of the page where σ_n is standard deviation of noise, M is the size of the operator, N is the width or height of the image, and $f(m,n)$ is the noise-free discrete image which can be approximated to an image showing a high signal-to-noise ratio (SNR) obtained by averaging some noisy images [8]. The large σ means that it can be much affected by Gaussian noise. For solving this problem, the $S_{4,4}$ is modified to a $4*4$ form consisting of a $2*2$ Z block and a $2*2$ $-Z$ block, which were repeated as shown in Fig. 6(a). The modified form

$$\sigma_{S_{4,4}} = \sqrt{\frac{50415\sigma_n^4}{N^2} + \frac{4\sigma_n^2}{N^4}\sum_{m=1}^{M+N}\sum_{n=1}^{M+N}\left[\mathbf{S_{4,4}(i,j)}^*\mathbf{S_{4,4}(i,j)}^* f(m,n)\right]^2} \tag{10}$$

$$\sigma_{\mathrm{EOL}} = \sqrt{\frac{1352\sigma_n^4}{N^2} + \frac{4\sigma_n^2}{N^4}\sum_{m=1}^{M+N}\sum_{n=1}^{M+N}\left[\mathbf{O}_{\mathrm{EOL}}(i,j)^*\mathbf{O}_{\mathrm{EOL}}(i,j)^* f(m,n)\right]^2} \tag{11}$$

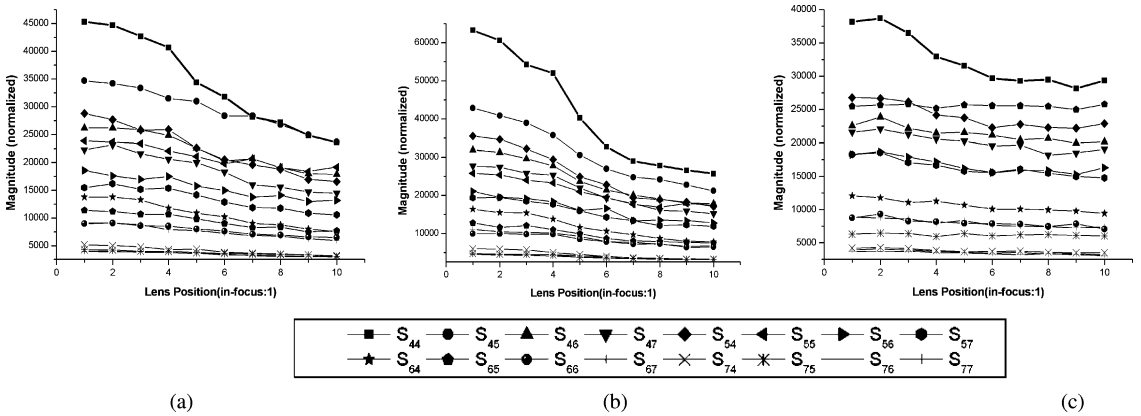

Fig. 5. Magnitude comparison of 16 ac components versus lens position. (a) Straw. (b) Sand. (c) Doll.

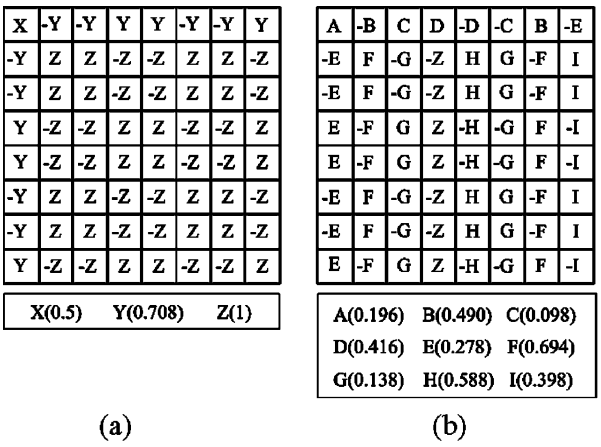

Fig. 6. Coefficient distributions for the DCT result components of $S_{4,4}$, $S_{4,5}$, and $S_{5,4}$. (a) $S_{4,4}$. (b) $S_{4,5}$ and $S_{5,4}^T$.

also has an advantage due to its symmetry. Based on the above considerations, the $4*4$ MF-DCT operator, $\mathbf{O_{MF\text{-}DCT}}$, is proposed as

$$\mathbf{O_{MF\text{-}DCT}}: \begin{bmatrix} 1 & 1 & -1 & -1 \\ 1 & 1 & -1 & -1 \\ -1 & -1 & 1 & 1 \\ -1 & -1 & 1 & 1 \end{bmatrix} \tag{12}$$

and the standard deviation for this operator is given by (13), shown at the bottom of the page.

The focus measure is thus computed by square of the convolution with $4*4$ image block $\mathbf{P}$ and an MF-DCT operator

$$FM_{\mathrm{MF-DCT}} = \sum_x \sum_y [\mathbf{P}_{x,y} * \mathbf{O_{MF\text{-}DCT}}]^2. \tag{14}$$

A comparison of the $S_{4,4}$ component and the proposed MF-DCT operator for three different images (without noise) is shown in Fig. 7. In all of the cases, MF-DCT shows the largest variation. In addition, the local maxima problem shown by the $S_{4,4}$ component in Fig. 7(c) is solved by using the MF-DCT. In this work, the evaluation window size is $40*40$. Hence, the focus measure is calculated by multiplying this evaluation window with a $4*4$ proposed operator as shown in Fig. 8(a).

B. Object Detection and Fuzzy Reasoning

For the object detection process, a multiple windows-based approach has been used in the present work. The focusing region has multiple windows (with size $40*40$), as shown in Fig. 8(a). When the lens moves from the first to the final step, the proposed operator calculates the in-focus lens position (or peak distance) corresponding to each window, as shown in Fig. 8(b). Assuming that the depth of each object is not significantly deep (resulting in each object having only one "peak distance," as calculated from the focus measure), objects can be classified by grouping several adjacent windows showing the same "peak distance" as shown in Fig. 8(c). Using the same procedure, the number of multiple windows belonging to the object (size) and the number of multiple windows belonging to the object and appearing in the center part (window counting in the center part) are calculated as shown in Fig. 8(d).

Then, target object selection is performed with the assumption that there is a high probability of the following:

$$\sigma_{MF\text{-}DCT} = \sqrt{\frac{1568\sigma_n^4}{N^2} + \frac{4\sigma_n^2}{N^4} \sum_{m=1}^{M+N} \sum_{n=1}^{M+N} [\mathbf{O_{MF\text{-}DCT}}(i,j) * \mathbf{O_{MF\text{-}DCT}}(i,j) * f(m,n)]^2} \tag{13}$$

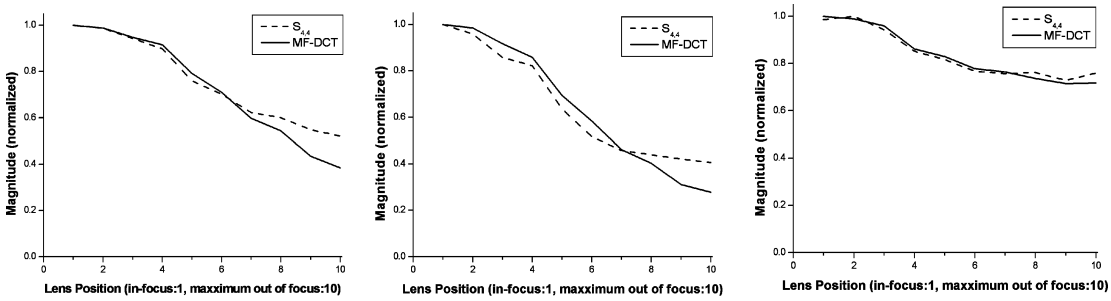

Fig. 7. Comparison of $S_{4,4}$ and MF-DCT (without noise). (a) Straw. (b) Sand. (c) Doll.

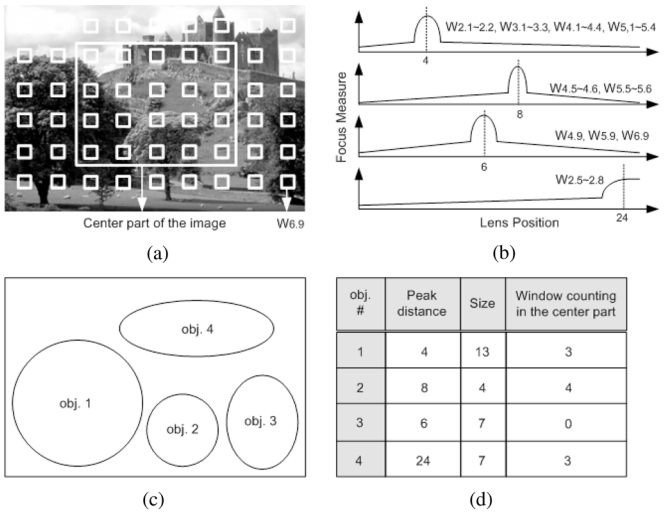

obj. #	Peak distance	Size	Window counting in the center part
1	4	13	3
2	8	4	4
3	6	7	0
4	24	7	3

Fig. 8. Object detection using multiple windows. (a) Sample image with multiple windows. (b) Detecting peak distance of each window. (c) Grouping of windows. (d) Extracting the information of each object.

1) the target object is positioned near the camera;
2) the target object occupies the center part of the image;
3) the size of the target object is large.

The distance of any object from the lens and its position in the scene are the important factors which help in the selection process. For instance, if object 1 is not only nearer to the camera lens but also occupies the center of the scene compared with object 2, then object 1 has more chances to be the target. In another case, if object 1 is in the center of the scene but located far from the camera and object 2 is out of the center but located near the camera, then target selection is ambiguous. To include all of the above considerations and conditions, a fuzzy reasoning-based approach [15], [16] is adopted for the target object selection process. Three membership functions, namely, "peak distance" $\mu_1(D)$, "window counting in the center part" $\mu_2(C)$ and "size" $\mu_3(S)$ are shown in Fig. 9 and given by

$$\mu_1(D) = \begin{cases} \frac{D}{d_1}, & D \le d_1 \\ 1 - \frac{D-d_1}{\max(D)}, & D > d_1 \end{cases} \tag{15}$$

$$\mu_2(C) = \begin{cases} \frac{C}{c_1}, & C \le c_1 \\ 1, & C > c_1 \end{cases} \tag{16}$$

$$\mu_3(S) = \frac{S}{\max(S)} \tag{17}$$

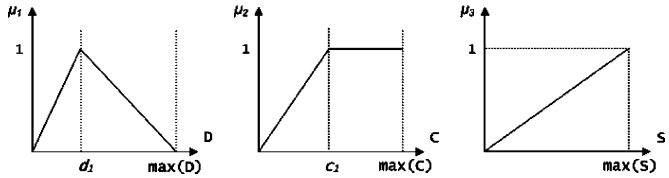

Fig. 9. Fuzzy membership functions.

where d_1 is the distance to avoid the obstacle which is located too close to the camera and c_1 is the threshold value of "window counting in the center part." The d_1 and c_1 can be varied with its application and camera parameter, but can be used as $d_1 = 1/5$ of $\max(D)$ and $c_1 = 1/2$ of $\max(C)$ for default. Each value is calculated from the object detection procedure, and fuzzy reasoning is performed by the following logic rules.

1) IF $\mu_1(D_1) * \mu_2(C_1)$ is bigger than $\mu_1(D_2) * \mu_2(C_2)$, THEN target distance is D_1.
2) IF $\mu_1(D_1) * \mu_2(C_1)$ is equal to $\mu_1(D_2) * \mu_2(C_2)$ AND S_1 is bigger than S_2, THEN target distance is D_1.

The large value of the membership function indicates that the object has a high probability to be the main object. In the logic rules, the multiplication operator is used in place of the sum operator because both μ_1 and μ_2 are important factors in selecting the target object. For example, multiplication of (0.5, 0.5) is higher than (0.8, 0.2) though the two sums are equal.

C. Two-Step Searching Strategy

The proposed AF method uses a two-step searching method to find the in-focused lens position effectively. If the distance between two consecutive lens positions is δ, at the first search, it searches by moving the lens with interval $I = n * \delta \ge AUM$ to reduce the searching time as well as to remove the effect of the AUM [7], [8] for effective object grouping. The first searching points are shown as

$$\textbf{\textit{Search-1 positions}} = \left\{ S_{(k-1)n+1} \,|k = 1 \ldots K \right\} \tag{18}$$

where $K = N/n$ and N is the total number of lens movable points as shown in Fig. 10. Assuming that the main object is detected at S_m, the second search proceeds around the position with the Search-2 positions

$$\left\lfloor S_m - \frac{I}{2} \right\rfloor \le \textbf{\textit{Search-2 positions}} \le \left\lceil S_m + \frac{I}{2} \right\rceil. \tag{19}$$

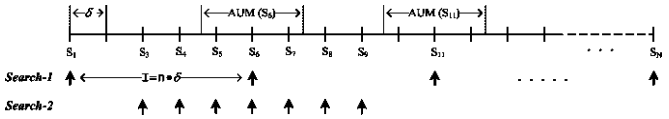

Fig. 10. Two-step search strategy when the main object is detected at S_6 through the first search with $n = 5$ and $\mathrm{AUM} = 2.8\delta$.

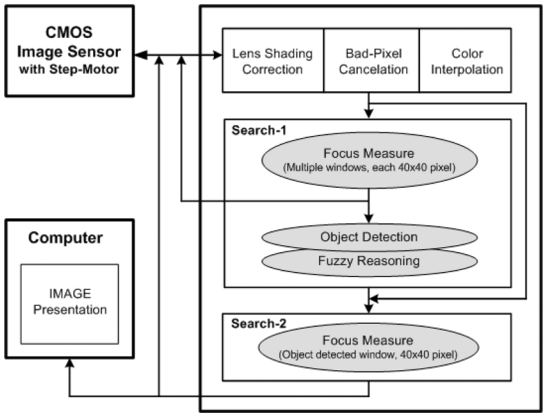

Fig. 11. Top-level block diagram of the proposed AF function.

IV. Hardware Implementation

The proposed AF algorithm is designed as a full digital block using Verilog HDL and fabricated with 0.35-μm CMOS technology through auto place and route with the Samsung standard cell library. The synthesized gate count is 1186 and placed with the size of 1182 $\times$ 1166 μm, including the macro memory. The top block diagram depicting the entire process of the AF function using the proposed algorithm is shown in Fig. 11.

The major functions shown in the diagram, namely, focus measure, object detection, and fuzzy reasoning and searching criteria have already been discussed in earlier sections. In the AF function, the power consumption is mainly due to the focus measure part [3] because it calculates the relation among all pixels using several adders and shifters. Therefore, we have tried to reduce the complexity of the block. The focus measure can be obtained by summing the convolutions of $\mathbf{O_{MF\text{-}DCT}}$ and $4*4$ pixel block, $\mathbf{P}$, through all pixels. The operator has the feature of a rotationally symmetric form: it makes the $1*4$ pixels to be shared four times. Thus, we made it slice, $\mathbf{S}$, as shown in Fig. 12, and the convolution can be implemented by pipeline as

$$\begin{aligned} FM_{\mathrm{MF-DCT}} = {} & \left|-(\mathbf{S_1}+\mathbf{S_2})+(-\mathbf{S_3}-\mathbf{S_4})\right|^2 \\ & +\left|-(-\mathbf{S_2}+\mathbf{S_3})+(-\mathbf{S_4}-\mathbf{S_5})\right|^2 \\ & +\left|-(\mathbf{S_3}+\mathbf{S_4})+(\mathbf{S_5}+\mathbf{S_6})\right|^2 \\ & +\left|-(\mathbf{S_4}+\mathbf{S_5})+(\mathbf{S_6}+\mathbf{S_7})\right|^2 \ldots \\ & +\left|-(\mathbf{S_{1597}}+\mathbf{S_{1598}})+(\mathbf{S_{1599}}+\mathbf{S_{1600}})\right|^2 \end{aligned}$$

where

$$\begin{aligned} \mathbf{S_{n(n\le 2)}} &= (\mathbf{P_{1,n}}+\mathbf{P_{2,n}})-(\mathbf{P_{3,n}}+\mathbf{P_{4,n}}) \\ \mathbf{S_{n(n\ge 3)}} &= (\mathbf{P_{\alpha+2,\beta}}+\mathbf{P_{\alpha+3,\beta}})-(\mathbf{P_{\alpha,\beta}}+\mathbf{P_{\alpha+1,\beta}}) \end{aligned}$$

where

$$\begin{aligned} \alpha &= \left\lfloor \frac{n}{w} \right\rfloor + 1 \\ \beta &= n\%w. \end{aligned} \tag{20}$$

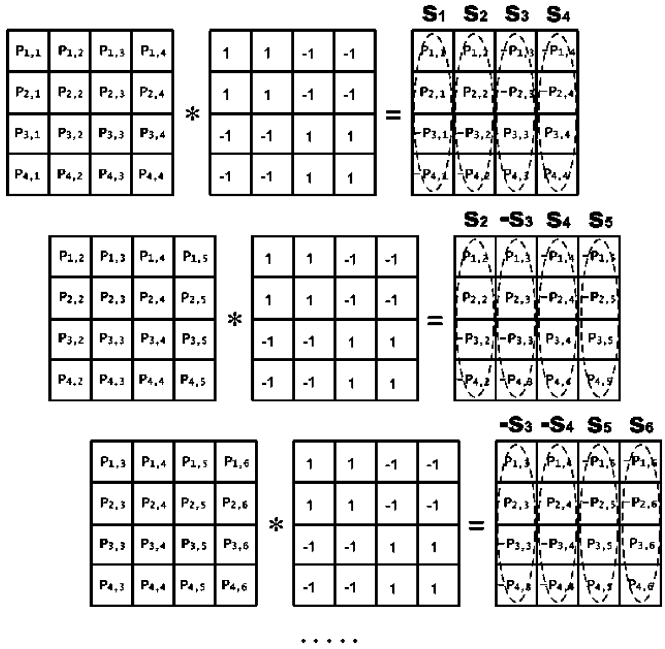

Fig. 12. Making a slice, $\mathbf{S_n}$, at the convolution operation.

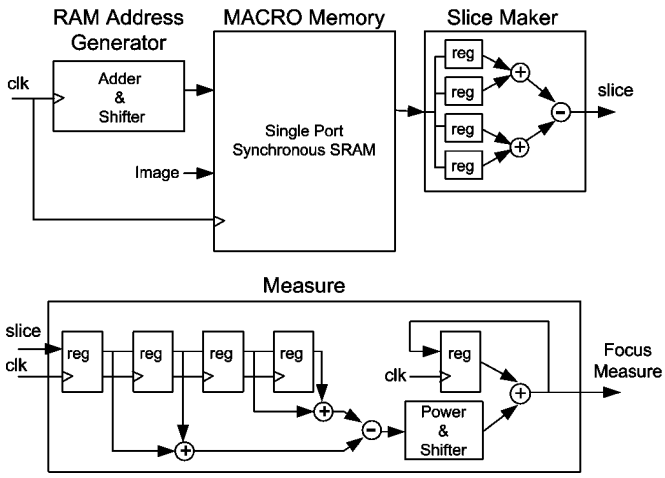

Fig. 13. Block diagram of the designed focus measure function.

The designed focus measure block is shown in Fig. 13. The image from the CMOS image sensor was saved at a single-port SRAM with the generated address, converted as a slice, and then entered to the pipeline for measure. The output is finally accumulated being powered and adjusted to the small size which was determined through register transfer level (RTL) simulation.

V. Experimental Result

A. Comparison of Focus Measure

AUM proposed by Subbarao and Tyan [7], [8] is a method for comparing the sensitivity of Gaussian noise of the different focus measures to select the optimal focus measuring operator. The AUM near the focused position is defined as follows:

$$\mathrm{AUM} = 2\delta\sqrt{\frac{2\sigma}{2\overline{\Gamma}_o - \overline{\Gamma}_+ - \overline{\Gamma}_-}} \tag{21}$$

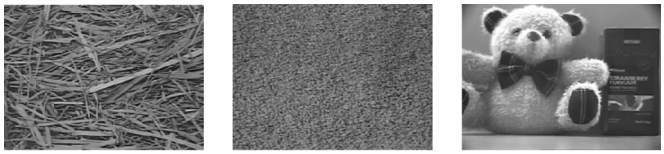

(a) (b) (c)

Fig. 14. Three in-focused sample objects A (Straw), B (Sand), and C (Doll). (a) Straw. (b) Sand. (c) Doll.

TABLE I
COMPARISON OF AUM

Object	Sobel	EOL	SML	FSWM	WT	MF-DCT	
	Exp.	Exp.	Exp.	Exp.	Exp.	Exp.	Theo.
A	1.61	2.12	0.52	2.49	0.65	0.42	0.59
B	2.15	1.27	0.55	2.43	0.61	0.59	0.51
C	2.66	3.30	1.02	1.29	0.83	0.68	0.99

* EOL = Energy of Laplacian, Exp.= experimental, Theo. = theoretical.

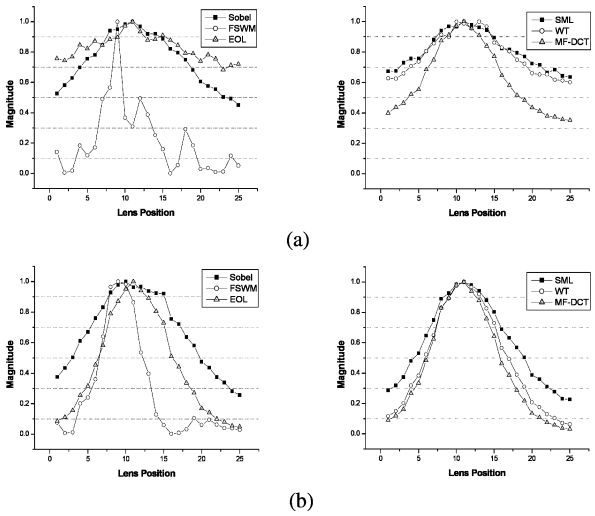

Fig. 15. Comparison of focus measure with object A: (a) with 5% impulsive noise and (b) without noise.

where $\overline{\Gamma}_-$, $\overline{\Gamma}_o$, and $\overline{\Gamma}_+$ are three focus measures near the focused position satisfying $\overline{\Gamma}_- < \overline{\Gamma}_o$ and $\overline{\Gamma}_+ < \overline{\Gamma}_o$, σ is the standard deviation of the operator, and δ is the distance between two consecutive lens position. $\overline{\Gamma}_-$ and $\overline{\Gamma}_+$ can be determined using the left-hand and right-hand values nearest the peak measure $(\overline{\Gamma}_o)$, and δ can be determined by the distance of consecutive optical zoom steps varied with the step motor of the camera. The AUM for the proposed operator is calculated using (13) and (21). For experimental measurement of AUM, three object samples A, B, and C, as shown in Fig. 14, are actually recorded ten times for various Gaussian noise at each 25 different lens positions. The comparison of AUM is summarized in Table I. It can be seen that MF-DCT shows the best performance for object A and C, and SML shows the best for object B. Also, WT is effective to Gaussian noise.

Another noise characteristic of concern is impulsive noise. For this, we added 5% salt and pepper noise to the 750 images with above sample objects, and the result of object A with 5% noise is shown in Fig. 15. In case of EOL and the FSWM 7-tap filter, they produce local maximum with 5% noise. WT and

TABLE II
COMPARISON OF VARIATION WITH 5% IMPULSIVE NOISE (UNIT: %)

Object	Sobel	EOL	SML	FSWM	WT	MF-DCT
A	55	31	36	100	40	65
B	58	21	41	98	35	64
C	32	15	24	100	19	34

* Variation is calculated by 1 minus the ratio of the minimum with the maximum measure.

TABLE III
COMPARISON OF LINEARITY WITH 5% IMPULSIVE NOISE (UNIT: %)

Object	Sobel	EOL	SML	FSWM	WT	MF-DCT
A	100	-	96	-	84	100
B	100	-	80	-	92	92
C	-	-	-	-	-	60

* Linearity is calculated by the ratio of the local maximum with total lens position.
* The '-' means the measure does not show linearity at all.

TABLE IV
COMPARISON OF VARIATION WITHOUT NOISE (UNIT: %)

Object	Sobel	EOL	SML	FSWM	WT	MF-DCT
A	74	95	77	100	94	97
B	86	97	84	98	97	93
C	88	72	68	76	84	88

TABLE V
COMPARISON OF LINEARITY WITHOUT NOISE (UNIT: %)

Object	Sobel	EOL	SML	FSWM	WT	MF-DCT
A	96	100	100	88	100	100
B	100	100	100	100	100	100
C	88	72	68	76	84	88

SML are not able to produce linear measures with 5% noise. For Sobel and MF-DCT, they satisfy monotonicity with both noise levels. It is obvious from Table I and Fig. 15(a) that the proposed MF-DCT shows excellent robustness with Gaussian and impulsive noise compared with other focus measures. Comparative studies of variation and linearity with 5% impulsive noise are shown in Tables II and III respectively. Although FSWM, MF-DCT, and Sobel show large variation, only MF-DCT shows good linearity for all objects. It is apparent from these tables that MF-DCT appears as a robust focus measure. Additionally, in the case of noise-free conditions, MF-DCT and WT record the best performances, although all of the operators show good performance on linearity and variations, as shown in Fig. 15(b) and Tables IV and V, respectively.

B. Object Detection and Fuzzy Reasoning

To compare the proposed searching algorithm (object detection and fuzzy reasoning with multiple windows) with traditional searching algorithms (center window-based), three cases are considered, as shown in Fig. 16, and MF-DCT is used for both searching algorithms. Traditional searching algorithms are not able to perform object detection. For the two cases, when

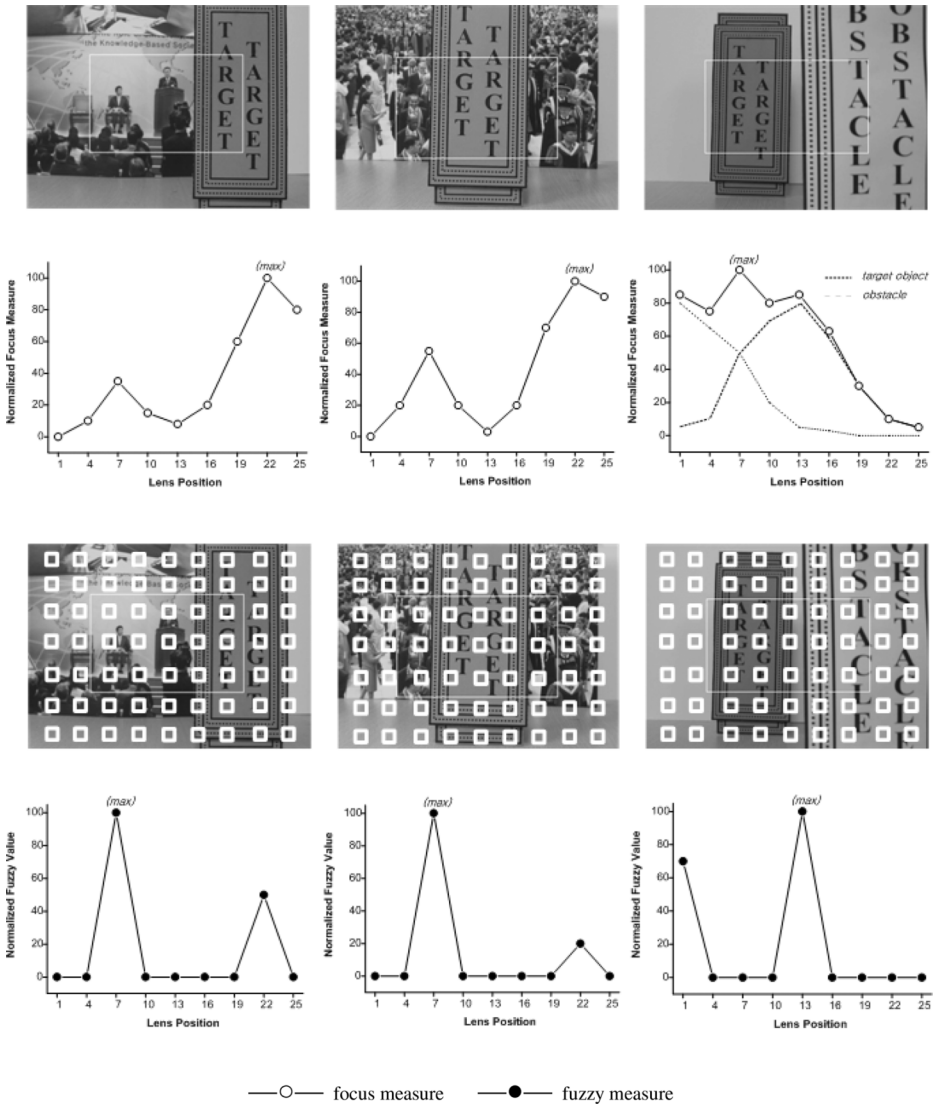

Fig. 16. Comparison of traditional and proposed searching algorithms. (a)–(c) Three test positions with center window. (d)–(f) Focus measure of (a)–(c) (traditional). (g)–(i) Three test positions with multiple windows. (j)–(l) Fuzzy measure of (g)–(i) (proposed).

when the target object is stepped aside the center window [Fig. 16(a) and (g)] and the background in the center window has more high-frequency contents than the target object even if the main object is in the center window [Fig. 16(b) and (h)], traditional AF algorithms focus on background located at the "22" lens position, as shown in Fig. 16(d) and (e), but the proposed AF algorithm distinguishes two objects (one labeled as TARGET, another in background) at "7" and "22" lens positions, respectively, and measures each fuzzy value as shown in Fig. 16(j) and (k). Then, it selects the "7" lens position as the target object which shows the maximum fuzzy measure. In another case, when two objects are positioned at the center window [Fig. 16(c) and (i)], traditional algorithms create a wrong and maximum focus measure at lens position "7" by summing each focus measure of two objects as shown in Fig. 16(f). With the proposed method, the creation of the false peak distance can be resolved by object detection. It detects two objects in lens positions "1" and "13," respectively, and then selects lens position "13" as the best focus distance as shown in Fig. 16(l). Even though the object labeled as "OBSTACLE" occupies half of the center window, it failed to get the good value of membership function μ_1 because it is located too close to the lens. Test environment and results for more objects are shown in Figs. 17 and 18, respectively. From these results, it is

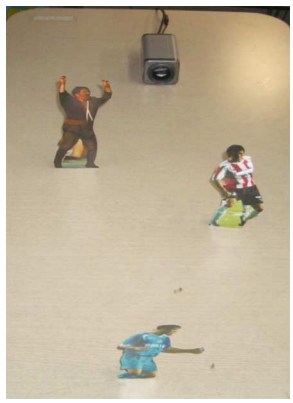

Fig. 17. Test environment for the comparison of traditional and proposed searching algorithms.

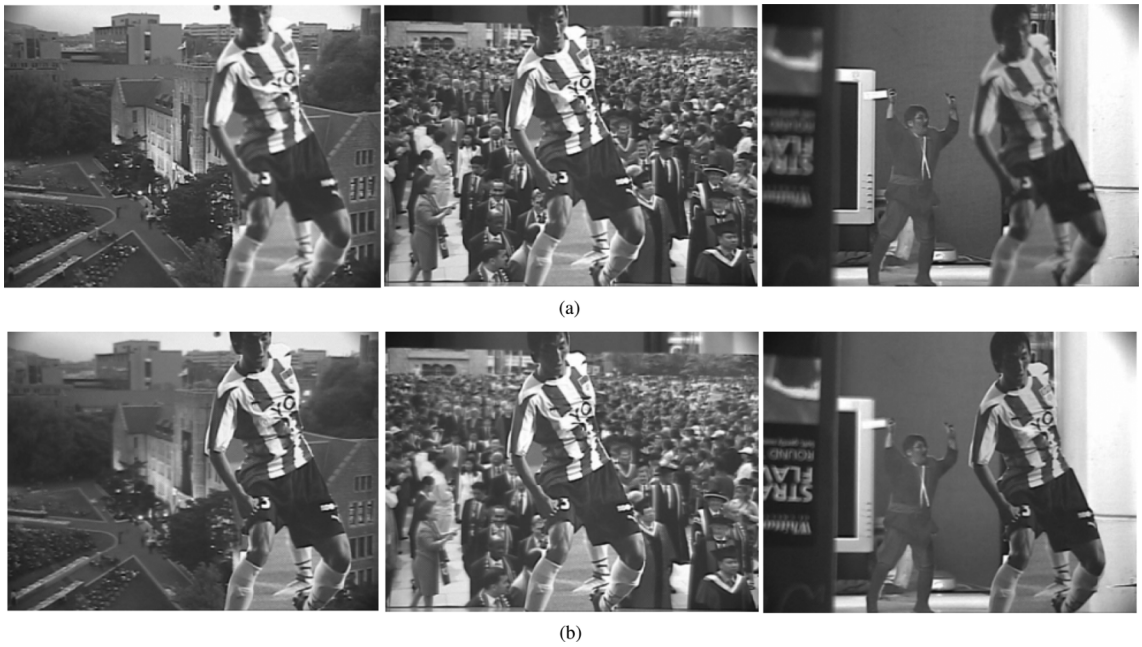

Fig. 18. Comparison of test results obtained with (a) traditional and (b) proposed searching algorithms.

obvious that the proposed algorithm can select the target object effectively and improves the quality of the digital image.

VI. Conclusion

This paper describes the focus measure operator and searching algorithm for an enhanced AF system. The presented focus measure is robust because it is derived from the MF-DCT component and the form is simple and rotationally symmetric. Also, the proposed searching strategy performs object detection and target selection using fuzzy reasoning. The AF algorithm is fabricated with a conventional CMOS process using a standard cell library. The experimental results verify that the proposed operator shows the best performance in response to Gaussian and impulsive noises compared with other operators, and the searching algorithm can improve the quality of the image by solving the frequently focus missing problems.

References

[1] S. M. Sohn, S. H. Yang, S. W. Kim, K. H. Baek, and W. H. Paik, "SoC design of an auto-focus driving image signal processor for mobile camera applications," *IEEE Trans. Consumer Electron.*, vol. 52, no. 1, pp. 10–16, Feb. 2006.

[2] V. Peddigari, M. Gamadia, and N. Kehtarnavaz, "Real-time implementation issues in passive automatic focusing for digital still cameras," *J. Imaging Sci. Technol. (IS&T)*, vol. 49, no. 2, pp. 114–123, Mar./Apr. 2005.

[3] E. Krotkov, "Focusing," *Int. J. Comput. Vis.*, vol. 1, pp. 223–237, 1987.

[4] K. Ooi, K. Izumi, M. Nozaki, and I. Takeda, "An advanced auto-focus system for video camera using quasi-condition reasoning," *IEEE Trans. Consumer Electron.*, vol. 36, no. 3, pp. 526–530, Aug. 1990.

[5] J. M. Tenenbaum, "Accommodation in Computer Vision," Ph.D. dissertation, Dept. of Comput. Sci., Stanford Univ., Stanford, CA, 1970.

[6] M. Subbarao, T. Choi, and A. Nikzad, "Focusing techniques," *J. Opt. Eng.*, vol. 32, no. 11, pp. 2824–2836, 1993.

[7] M. Subbarao and J. K. Tyan, "The optimal focus measure for passive autofocusing and depth-from-focus," in *Proc. SPIE. Videometrics IV*, Oct. 1995, pp. 89–99.

[8] M. Subbarao and J. K. Tyan, "Selecting the optimal focus measure for autofocusing and depth-from-focus," *IEEE Trans. Pattern Anal. Mach. Intell.*, vol. 20, no. 8, pp. 864–870, Aug. 1998.

[9] S. K. Nayar and Y. Nakagawa, "Shape from focus," *IEEE Trans. Pattern Anal. Mach. Intell.*, vol. 16, no. 8, pp. 824–831, Aug. 1994.

[10] K. S. Choi, J. S. Lee, and S. J. Ko, "New autofocus technique using the frequency selective weighted median filter for video cameras," *IEEE Trans. Consumer Electron.*, vol. 45, no. 3, pp. 820–827, Aug. 1999.

[11] M. Charfi, A. Nyeck, and A. Tosser, "Focusing criterion," *Electron. Lett.*, vol. 27, no. 14, pp. 1233–1235, Jul. 1991.

[12] G. Yang and B. J. Nelson, "Wavelet-based autofocusing and unsupervised segmentation of microscopic images," in *Proc. IEEE/RSJ Int. Conf. Intelli. Robots Syst.*, Oct. 2003, pp. 2143–2148.

[13] J. Kautsky, J. Flusser, B. Zitova, and S. Simberova, "A new wavelet-based measure of image focus," *Pattern Recognit. Lett.*, vol. 23, no. 14, pp. 1785–1794, Dec. 2002.

[14] J. He, R. Zhou, and Z. Hong, "Modified fast climbing search autofocus algorithm with adaptive step size searching technique for digital camera," *IEEE Trans. Consumer Electron.*, vol. 49, no. 2, pp. 257–262, May 2003.

[15] C. Han, W. S. Kerwin, T. S. Hatsukami, J.-N. Hwang, and C. Yuan, "Detecting objects in image sequences using rule-based control in an active contour model," *IEEE Trans. Biomed. Eng.*, vol. 50, no. 6, pp. 705–710, Jun. 2003.

[16] K. H. Lee, *First Course on Fuzzy Theory and Applications*. Berlin, Germany: Springer-Verlag, 2004.

[17] A. S. Malik and T. S. Choi, "Consideration of illumination effects and optimization of window size for accurate calculation of depth map for 3-D shape recovery," *Pattern Recogn.*, vol. 40, no. 1, pp. 154–170, Jan. 2007.

Sang-Yong Lee received the B.S. degree in computer engineering from Korea Aerospace University, Kyungi, Korea, in 2001 and the M.S. degree in electronics and computer engineering from Korea University, Seoul, Korea, in 2003, where he is currently working toward the Ph.D. degree in electronics and computer engineering.

His research interests include digital video/image processing, sigma-delta audio AD/DAC, and system-on-chip.

Yogendera Kumar was born in Hardwar, India, on December 5, 1972. He received the Ph.D. degree from the Indian Institute of Technology, Roorkee, India (IITR) in 2002.

He was a Post-Doctoral Researcher with IITR and the Emerging Technologies Research Centre, De Montfort University, Leicester, U.K. In February 2003, he joined the Department of Electrical and Electronics Engineering, Birla Institute of Technology and Science, Pilani, Rajasthan, India, as a faculty member. He is currently a Visiting Professor with the Department of Electronics Engineering, Korea University, Seoul, Korea. He also served as a Visiting Professor with the Indian Institute of Information Technology and Management, Gwalior, India. His research interests are GaAs VLSI design, VLSI Interconnect design, network-on-chip design, and image processing.

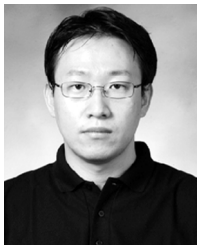

Ji-Man Cho received the B.S. degree from Myoung Ji University, Korea, in 1997 and the M.S. degree in material science and engineering from Korea University, Seoul, Korea, in 1999, both in material science and engineering . He is currently working toward the Ph.D. degree in electronics and computer engineering at Korea University.

His research interests include MEMS inertial sensor and interface signal processing for microsensor applications.

Sang-Won Lee received the B.S. and M.S. degrees in electronics engineering and the Ph.D. degree from Korea University, Seoul Korea, in 1989, 1991, and 2001, respectively.

He was with LG Electronics, Seoul, Korea, from 1991 to 1997. After completing his doctoral work, he was a Chip Verification Engineer with Advanced Micro Devices Inc. Presently, he is a Chip Micro Architect with Intel Corporation, Hudson, MA. His research interests are microprocessor architecture, system interconnect design, systems-on-chip, and low-power digital system design.

Soo-Won Kim received the B.S. degree in electronics engineering from Korea University, Seoul, Korea in 1974, and the M.S. and Ph.D. degrees in electrical engineering from Texas A&M University, College Station, in 1983 and 1987, respectively.

He joined the Department of Electronics Engineering, Korea University, as an Assistant Professor in 1987. Since 1989, he has been a Professor with the Department of Electronics Engineering, Korea University. His areas of interest are design of mixed-mode ICs, RF PLLs, and high-speed and low-power digital systems.